NeuroImage 206 (2020) 116338

Contents lists available at ScienceDirect

NeuroImage

journal homepage: www.elsevier.com/locate/neuroimage

Multi-band SWIFT enables quiet and artefact-free EEG-fMRI and awake fMRI studies in rat

Jaakko Paasonen [a], Hanne Laakso [a,b], Tiina Pirttimäki [a,c], Petteri Stenroos [a], Raimo A. Salo [a], Ekaterina Zhurakovskaya [a,b], Lauri J. Lehto [a,b], Heikki Tanila [a], Michael Garwood [b], Shalom Michaeli [b], Djaudat Idiyatullin [b], Silvia Mangia [b], Olli Gröhn [a,*]

[a] A. I. Virtanen Institute for Molecular Sciences, University of Eastern Finland, Kuopio, Finland
[b] Center for Magnetic Resonance Research, University of Minnesota, Minneapolis, MN, USA
[c] Department of Psychology, University of Jyväskyla, Jyväskyla, Finland

ARTICLE INFO

Keywords:
Awake
Electroencephalography
Functional connectivity
Functional magnetic resonance imaging
Rats

ABSTRACT

Functional magnetic resonance imaging (fMRI) studies in animal models provide invaluable information regarding normal and abnormal brain function, especially when combined with complementary stimulation and recording techniques. The echo planar imaging (EPI) pulse sequence is the most common choice for fMRI investigations, but it has several shortcomings. EPI is one of the loudest sequences and very prone to movement and susceptibility-induced artefacts, making it suboptimal for awake imaging. Additionally, the fast gradient-switching of EPI induces disrupting currents in simultaneous electrophysiological recordings. Therefore, we investigated whether the unique features of Multi-Band SWeep Imaging with Fourier Transformation (MB-SWIFT) overcome these issues at a high 9.4 T magnetic field, making it a potential alternative to EPI. MB-SWIFT had 32-dB and 20-dB lower peak and average sound pressure levels, respectively, than EPI with typical fMRI parameters. Body movements had little to no effect on MB-SWIFT images or functional connectivity analyses, whereas they severely affected EPI data. The minimal gradient steps of MB-SWIFT induced significantly lower currents in simultaneous electrophysiological recordings than EPI, and there were no electrode-induced distortions in MB-SWIFT images. An independent component analysis of the awake rat functional connectivity data obtained with MB-SWIFT resulted in near whole-brain level functional parcellation, and simultaneous electrophysiological and fMRI measurements in isoflurane-anesthetized rats indicated that MB-SWIFT signal is tightly linked to neuronal resting-state activity. Therefore, we conclude that the MB-SWIFT sequence is a robust preclinical brain mapping tool that can overcome many of the drawbacks of conventional EPI fMRI at high magnetic fields.

1. Introduction

Functional MRI (fMRI) studies in animal models provide invaluable information regarding normal and abnormal brain function. When fMRI is combined with optical and/or electrical recording and stimulation techniques, multiple spatial and temporal scales of brain network activity can be assessed and manipulated. This allows for investigations of complex central nervous system functions and disease mechanisms, and can facilitate the search for biomarkers of disease progression and treatment response.

Combining complex experimental setups with fMRI, however, is not straightforward. Surgical manipulations of the skull and implantation of measuring or stimulation instruments can induce strong magnetic susceptibility differences in the brain, leading to severe B_0 field distortions that are difficult or impossible to compensate for or correct (In et al., 2017). As rodent fMRI studies are typically performed with the echo planar imaging (EPI) pulse sequence at high magnetic fields, inhomogeneities of the B_0 field significantly affect the image quality, and are commonly observed as geometric deformations and signal drop-outs. Additionally, the rapidly switching strong gradients in the EPI

Abbreviations: BOLD, blood oxygenation level dependent; EEG, Electroencephalography; EPI, echo planar imaging; FC, functional connectivity; FOV, field of view; FSEMS, fast spin echo multi slice; HRF, hemodynamic response function; IC, independent component; ICA, independent component analysis; ID, inner diameter; MB-SWIFT, Multi-Band SWeep Imaging with Fourier Transformation; SE, spin echo; SPL, sound pressure level.

* Corresponding author. A.I.V. Institute for Molecular Sciences, University of Eastern Finland, P.O. Box 1627, FI-70211, Kuopio, Finland.
E-mail address: olli.grohn@uef.fi (O. Gröhn).

https://doi.org/10.1016/j.neuroimage.2019.116338
Received 20 August 2019; Received in revised form 18 October 2019; Accepted 4 November 2019
Available online 12 November 2019

sequence create strong acoustic noise and can cause severe artefacts in complementary recording techniques such as electroencephalography (EEG).

Another major issue in animal fMRI studies is anesthesia, which is used to minimize the stress and movement of the animals (Lukasik and Gillies, 2003). Anesthesia heavily modulates brain function and subsequently the outcome of both stimulation (Huttunen et al., 2008; Paasonen et al., 2016, 2017; Sommers et al., 2009) and resting-state fMRI experiments (Grandjean et al., 2014; Jonckers et al., 2014; Paasonen et al., 2018), making it perhaps the biggest confounding factor in animal fMRI experiments.

To overcome the effects of anesthesia, awake rodent imaging protocols have been introduced (King et al., 2005; Lahti et al., 1998; Stenroos et al., 2018). Despite careful habituation protocols and tight head fixation, however, completely motion-free data is rarely acquired. Part of the issue may be the EPI sequence, which is one of the loudest MRI sequences and may cause additional discomfort for the rats. The subsequent spontaneous body movement induces changes in B_0, which extend into the brain and induce deformations in the B_0-sensitive EPI images.

Recently, we introduced Multi-band SWeep Imaging with Fourier Transformation (MB-SWIFT) fMRI in the context of deep brain stimulation of the rat, and acquired fMRI responses comparable to those obtained with spin-echo (SE) EPI with minimal susceptibility artefacts from a tungsten wire electrode implanted into the ventral posteromedial nucleus of the thalamus (Lehto et al., 2017). MB-SWIFT is a three-dimensional radial MRI pulse sequence with large excitation and acquisition bandwidths, practically zero echo time, and minimal gradient switching steps during data acquisition (Idiyatullin et al., 2006; Idiyatullin et al., 2015). It is worth mentioning that the multi-band in the context of MB-SWIFT does not refer to the excitation of multiple slices (Moeller et al., 2010), but to multiple side bands of the excitation profile in readout dimension (Idiyatullin et al., 2015).

Interestingly, the functional signal-to-noise ratio appears to be higher in MB-SWIFT than in SE-EPI (Lehto et al., 2017). As MB-SWIFT is not sensitive to susceptibility-induced $T_2(*)$ effects, the fMRI contrast does not rely on the traditional blood oxygenation level-dependent (BOLD) effect (Ogawa et al., 1990), and likely originates from the in-flow effect of the cerebral blood (Lehto et al., 2017). Because of the sensitivity to blood in-flow, the method is also sensitive to MRI coil geometry. Additionally, the near zero echo time leads to sensitivity to most materials with hydrogens in the range of the radio frequency coils.

As a continuation of our previous study, the aim of this work was to assess whether the unique features of MB-SWIFT can be exploited in rat fMRI experiments to overcome many of the limitations associated with traditional EPI fMRI studies. The small gradient steps of MB-SWIFT should decrease the acoustic scanner noise and minimize the artefacts in simultaneous electrophysiological recordings, while the large bandwidth and near-zero echo time should make the images insensitive to B_0-distortions, originating from, e.g., movement, EEG electrodes, and air cavities. We further investigated whether the functional connectivity (FC) maps obtained from awake and isoflurane-anesthetized rats were comparable to those obtained in previous EPI studies, and how well MB-SWIFT signal correlates with neuronal activity by conducting simultaneous EEG-fMRI recordings.

2. Materials and methods

Animal procedures were approved by the Animal Experiment Board in Finland, and conducted in accordance with the European Commission Directive 2010/63/EU guidelines. In total 13 adult (418 ± 23 g) male Wistar rats (RccHan®:WIST; Envigo RMS B.V., Horst, Netherlands) were used in the experiments. The animals were individually-housed and maintained on a 12/12 h light-dark cycle at 22 ± 2 °C with 50%–60% humidity. Food and water were available *ad libitum*.

2.1. Magnetic resonance imaging

All MRI data were acquired in a high-field 9.4 T/31 cm bore magnet interfaced with an Agilent DirectDRIVE console (Palo Alto, CA, USA) using a custom-made (either in-house made or by Neos Biotec, Pamplona, Spain) surface transmit-receive radio frequency coil with a 22-mm inner diameter (ID). The materials of the custom-made coils (e.g., polytetrafluoroethylene) were selected so as not to be visible in the MB-SWIFT images. Animal holder parts were made of polyoxymethylene, which is slightly visible in the MB-SWIFT images.

All imaging except during the controlled body movement experiment was performed with a 12-cm ID gradient coil set. To allow more room for movement, the controlled body movement experiments were conducted in a larger 21-cm ID gradient coil set with slightly different MRI sequence parameters (values in parentheses below).

Anatomical images were acquired using a fast spin echo (SE) multi-slice (FSEMS) sequence with the following parameters: TR 3000 (3200) ms, echo spacing 12 ms, effective TE 48 ms, number of echoes 8, averages 4, bandwidth 62.5 kHz, matrix size 256×256 cm^2, field of view (FOV) 3.5×3.5 (4.0×4.0) cm^2, and 20–30 slices with a 0.5–1.0 mm thickness.

A multi gradient echo sequence was used to obtain B_0 field maps. The parameters were as follows: TR 1000 ms, TE 3.3 ms, echo spacing 2.1 ms, echoes 5, flip angle 60°, bandwidth 100 kHz, FOV 4.0×4.0 cm^2, and 5 slices with 1.0-mm thickness.

MB-SWIFT fMRI data were acquired with the following parameters: TR 0.97 ms, 2000 spokes per volume resulting in a temporal resolution of ~2 s, excitation/acquisition bandwidths 192/384 kHz, matrix size 64^3, FOV $3.5 \times 3.5 \times 6.4$ ($4.0 \times 4.0 \times 6.4$) cm^3, and flip angle 6°.

SE-EPI data were acquired with the following parameters: TR 2–4 s, TE 35 ms, bandwidth 208 kHz, matrix size 64×64 (64×32), FOV 3.5×3.5 (4.0×4.0) cm^2, and 8–15 slices with 1.5-mm thickness.

The lengths of the fMRI scans were as follows: 750 vol (25 min) for the awake resting-state fMRI measurements, 165 vol (5.5 min) for the controlled body movement experiments, and 300 vol (10 min) for the simultaneous electrophysiological and fMRI resting-state measurements of anesthetized rats.

During MRI, a warm water circulation system (Corio CD, Julabo, Seelbach, Germany) was used to keep the animals warm (~37 C°). Small animal physiology monitoring equipment (Model 1025, Small Animal Instruments Inc., New York, NY, USA) was used to follow the respiration rate. Temperature of the anesthetized rats was monitored with a rectal probe. Additionally, an MRI-compatible video camera (12M-i, MRC Systems GmbH, Heidelberg, Germany) was attached to the animal cradle to track the movement of the rats during the awake and controlled body movement experiments.

2.2. Sound pressure level measurements

Acoustic scanner noise levels inside the magnet bore were measured using an omnidirectional condenser microphone (MT830R, Audio-Technica Limited, Leeds, UK), attached to an audio interface (Scarlett 2i2, Focusrite Audio Engineering, High Wycombe, UK), and recorded with a PC and Audacity software (version 2.3.0, https://www.audacityteam.org/).

The system was calibrated by playing recorded MRI sounds through a loudspeaker (JBL LSR308, Harman International Industries, Stamford, CT, USA). Peak pressures ranging from 59 to 119 dB were recorded simultaneously with a sound pressure level (SPL) meter (Type 2232, Brüel & Kjær, Nærum, Denmark) and the MTR830R microphone. The SPL meter used A-weighting. The calculated SPL calibration curve for the microphone was highly linear ($R^2 = 0.998$).

In the MRI SPL measurements, the microphone was attached at a location near the rat head during *in vivo* measurements. The experiment was repeated 5–10 times with slightly different microphone positions (e.g., left side, right side, top, behind, front, etc.) for each pulse sequence – SE-EPI with 8 and 15 slices, and MB-SWIFT. Additionally, the

background noise levels were measured.

2.3. Controlled movement during EPI and MB-SWIFT

To determine the effect of body movement on fMRI images, it is necessary to prevent head-movement. Surgery was performed in one rat to attach a custom-made chronic implant directly on the skull to secure head fixation.

For surgery, the rat was anesthetized with isoflurane (Attane vet 1000 mg/g, Piramal Healthcare UK Limited, Northumberland, UK; 5% induction and 2% maintenance) in a mixture of N_2/O_2 70%/30%, and placed into a stereotaxic frame (David Kopf Instruments, Tujunga, CA, USA). The scalp was removed from top of the skull, and the skull was cleaned with sterile saline and hydrogen peroxide (3%). Small holes penetrating the dense compact bone layer were drilled throughout the skull to facilitate bone cement adhesion (Palacos R + G, Heraeus Medical, Hanau, Germany). After the bone cement dried (~10 min), a layer of dental cement (Selectraplus, DeguDent GmbH, Hanau, Germany) was applied. Two plastic pins (2 mm diameter, separated by 12 mm) aligned in left-right direction and covered with heat-shrinkable tubes were fixed on top of the dental cement layer, and final layers of dental cement were molded around the pins. After the cement dried, the pins were removed, leaving two holes in the implant for head-fixation. Buprenorphine (0.03 mg/kg s.c.; Temgesic, Indivior Europe Ltd, Dublin, Ireland) was given for postoperative pain and saline (10 ml/kg/day s.c.) was given to prevent dehydration. Injections were continued for 2 days twice daily, and the recovery and welfare of the rat were monitored closely.

After a recovery period of 1 week, the rat was anesthetized for an fMRI experiment with isoflurane (5% induction and 1.3–2.0% maintenance) to maintain the respiration rate at approximately 60 breaths per minute. A commercially available harness for rodents (TRIXIE Heimtierbedarf GmbH & Co. KG, Tarp, Germany) was placed on the anesthetized rat, and strings were attached to the posterior parts of the harness. In combination with a custom-made MRI holder including a head-fixation system compatible with an open loop radio frequency coil, the strings allowed us to remotely lift the body of the rat inside the bore. A breathing sensor was pushed inside the harness to monitor the depth of anesthesia. The head was fixed using an in-house made head-fixation system, including two pins going through the implant. Visual inspection was performed to ensure that the body movement induced by pulling the strings did not move the head and did not alter the tuning and matching of the radio frequency coil.

After the animal preparation and initial MRI adjustment steps, the controlled body movement fMRI experiments were performed. A block-model paradigm consisting 30 vol (60 s) of baseline and 15 vol (30 s) of controlled movement was used. The paradigm was repeated three times within one scan, resulting in a total of 165 vol (5.5 min). The scan was repeated three times with both MB-SWIFT and SE-EPI fMRI sequences. The B_0 maps were acquired from one rat in different body positions. After finishing the experiments, the rat was returned to its cage.

The whole fMRI experiment was repeated with the same rat after a 1-week rest period, resulting in a total of 12 fMRI scans (6 with each sequence).

2.4. Awake functional MRI with MB-SWIFT

The awake protocol is described in our previous report (Stenroos et al., 2018). Briefly, nine rats went through a 4-day habituation protocol before the awake fMRI. Each day, the rat was first anesthetized with isoflurane (5% induction and 2% maintenance in the same N2/O2 70%/30% mixture). The paws were secured with masking tape, and the body was gently wrapped with a plastic foam sheet. Silicone plugs were inserted into the ear cavities for hearing protection. The rat was transferred to an MRI holder and the head was fixed with a custom-made padded restraint kit. The holder was pushed into a mock scanner, isoflurane was set to zero, and the sounds of the fMRI protocol were played through a loudspeaker. The audio recording/playback system was the same as described in section 2.1.

The length of the habituation session was increased in 10-min increments, starting from 15 min on the first day, up to 45 min on day 4. The length of the resting-state fMRI measurement on the day 5 was 25 min. The imaging was started when the breathing rate reached ~110 breaths per minute, indicating a conscious condition. After habituation or imaging, isoflurane was increased gradually to 2%–3%, and the rat was released from restraint back to its cage. Chocolate cereal was given before and after the training as a reward.

2.5. Simultaneous EEG and fMRI measurements

To investigate the image distortions and the magnitude of gradient switching artefacts of MB-SWIFT and SE-EPI during simultaneous intracranial EEG and fMRI measurements, three rats underwent a surgery for acute electrode implantation prior to MRI. Additionally, the correlation between EEG and MB-SWIFT fMRI signals under isoflurane anesthesia was studied.

EEG was recorded with epidural electrodes made of polytetrafluoroethylene insulated silver wire (0.2 mm bare wire diameter, nominal outer diameter of coated wire 0.27 mm; AG549511, Advent Research Materials, Oxford, UK). The electrode tip was exposed for a 2-mm length and bent into an L-shape. The ground electrode comprised 20 mm of bare wire that was placed under the skin in the neck.

The rat was initially anesthetized with isoflurane as described in section 2.3. The skull was exposed and carefully cleaned and dried. The silver wire electrodes were implanted bilaterally on the dura over the somatosensory (S1) cortex (AP −2.12; ML 2.5) through small craniotomies. Similarly, the reference electrode was placed on the dura over the cerebellum. The intracranial electrodes were attached to the skull with cyanoacrylate glue.

After finishing the electrode implantation, the functionality of the electrodes was tested, and the rat was immediately transferred to an MRI holder for imaging. EEG was measured and recorded with an MRI-compatible BrainAmp MR system (5 kHz sampling rate; Brain Products GmbH, Gilching, Germany) equipped with a preamplifier (10x amplification; Multi Channel Systems, Reutlingen, Germany). The isoflurane concentration (1.3%–2.0%) during simultaneous fMRI and EEG data acquisition was adjusted to induce a clear burst-suppression state (Liu et al., 2011) monitored by EEG. After finishing the measurements, the rats were anesthetized with 5% isoflurane and then killed by cervical dislocation.

2.6. Data processing and analysis

The audio data were analyzed using Audacity and MATLAB (R2011a and R2017b; Mathworks Inc., Natick, MA, USA). As many hearing-related parameters, such as loudness, have a logarithmic nature, linear averages for peak and mean dB levels across the measurements were calculated.

The MB-SWIFT data were first reconstructed with SWIFT package 2018 (https://www.cmrr.umn.edu/swift/index.php) using correlation, gridding, and three iterations of the FISTA algorithm (Beck and Teboulle, 2009). The reconstruction time for one 3D volume was roughly 0.5–1.0 s while using a workstation (Celsius R970, Fujitsu, Tokyo, Japan). From each MB-SWIFT fMRI data-set, the first three volumes were discarded as the signal was reaching a steady-state. Subsequently, all MRI data were written to NIfTI using Aedes (http://aedes.uef.fi).

A single loop receiver coil was used for all measurements, and thus the fMRI images had a strong B_1 intensity gradient. This hampered the motion correction of MB-SWIFT awake rat fMRI data. Therefore, the intensity bias was removed from the images using an N4ITK bias correction (Tustison et al., 2010) with 4th order splines for the local reference image and 2nd order splines for the separate fMRI volumes. The bias-corrected volumes were motion corrected using Advanced

Normalization Tools (ANTs, http://stnava.github.io/ANTs/) (Avants et al., 2011). The acquired motion correction transformations were then applied to the original MB-SWIFT fMRI data sets. Three nuisance regressors for both translation and rotation were also computed from the motion correction transformation matrices.

For group-level analyses, the fMRI data were co-registered. Because MB-SWIFT fMRI images have low anatomical contrast, we used an indirect approach. The anatomical FSEMS images of each subject were first co-registered to a reference FSEMS volume with ANTs using affine and non-linear SyN registrations. Next, the acquired transformations were applied to the MB-SWIFT fMRI data sets. Finally, data were spatially smoothed (0.5 mm full-width at half-maximum Gaussian kernel) using SPM8 (www.fil.ion.ucl.ac.uk/spm).

Prior to the analysis of the awake rat MB-SWIFT fMRI data, volumes including movement were discarded. Exclusion was based on combined visual inspection of the image mass center (>0.1 voxels) and visible image displacement throughout the time series in raw data. Data periods containing less than continuous 45 motion-free volumes (1.5min) were also excluded. The amount of movement events was calculated as described earlier (Stenroos et al., 2018).

The effect of controlled body movement on fMRI voxels in the brain was analyzed with a block-design general linear model available in Aedes. Data-driven independent component analysis (ICA; FSL MELODIC, https://fsl.fmrib.ox.ac.uk/fsl/fslwiki/MELODIC) was used for the investigation of FC. Brain masks were drawn manually and used unless stated otherwise. Components that were located in big vessels, located only at surfaces, not bilateral, or anatomically poorly localized were excluded from the results to minimize the inclusion of non-neural components. The number of components for awake rat data (30) was chosen based on previous awake rat studies, in which 20–40 components were used, e.g., (Becerra et al., 2011; Liang et al., 2011). For isoflurane-anesthetized rats, fewer components (20) were selected because the isoflurane-induced cortical burst-suppression activity, which we aimed to detect, occurs throughout the cortex (Liu et al., 2011) and is easily detectable with low number of components.

For awake rat data, partial correlation coefficients were calculated between regions of interest defined by the obtained ICs (thresholded by MELODIC). The original MB-SWIFT signal was band-pass filtered at 0.01–0.15 Hz. Motion correction parameters and the brain volume global signal were used as nuisance regressors to minimize the residual effect of movement. For each subject, motion-free time series were divided into continuous 100 vol series, from which correlation values were averaged, and left-over data that did not fit the 100-vol limit were discarded. Fisher transformation to Z-scores was applied prior to averaging of correlation coefficients.

EEG data were inspected and analyzed using MATLAB and Spike2 (CED Ltd, Cambridge, England). Data were denoised from gradient switching artefacts using a wavelet-ICA method (Sheoran et al. 2014). Briefly, a discrete stationary wavelet decomposition was applied (MATLAB *swt*-function, mother wavelet sym8 at decomposition level 15) and then a fast ICA algorithm (https://research.ics.aalto.fi/ica/fastica/) was used to obtain ICs from the resulting wavelets. The components containing artefacts were manually selected and removed. Finally, an inverse discrete stationary wavelet transform was applied to recover the artefact-free data.

Subsequently, the denoised EEG data were band pass-filtered (0.05–15 Hz). The envelope of the signal was calculated using the absolute value of a Hilbert transformation. The data were then convolved with the hemodynamic response function (HRF) for anesthetized rats (Silva et al., 2007), and down-sampled to the MRI temporal resolution (0.5 Hz).

To minimize the effect of non-neuronal fluctuations in the EEG-fMRI correlation analysis, ICA was used to extract the fMRI time series for the isoflurane-induced cortical activity (Liu et al., 2011), which was subsequently compared with the cortical HRF-convolved EEG envelopes. Both MB-SWIFT and EEG data were detrended and median normalized, and the signals were aligned by maximizing cross-correlation. In sliding window analysis, to investigate the temporal stability of the EEG-fMRI correlation, correlations were calculated with 50 vol windows and 10 vol steps.

The threshold for statistical significance was set to $p < 0.05$. Statistical tests were performed with either analyzing software described above or MATLAB. All group-level values in the text and figures are represented as mean ± standard deviation. Data and codes are available upon request.

3. Results

3.1. Acoustic measurements

The results of the acoustic scanner noise measurements are summarized in Fig. 1. One of the most important observations was that the peak SPL (84.9 ± 1.7 dB) was dramatically lower ($p < 10^{-9}$, two-tailed Student's *t*-test) when measured during MB-SWIFT than when measured during the 8- and 15-slice EPI sequences (116.9 ± 0.6 dB and 116.8 ± 0.7 dB, respectively). The average SPL of MB-SWIFT (63.6 ± 1.7 dB) was also clearly lower than that of both the 8-slice (72.0 ± 5.4 dB, $p = 0.005$) or 15-slice (83.3 ± 4.3 dB, $p = 10^{-5}$) EPI sequences (two-tailed Student's *t*-test). There was also a significant increase (11.3 dB) in the average SPL during SE-EPI when the slice number was increased from 8 to 15 ($p = 0.001$, two-tailed Student's *t*-test).

If considering a 6-dB increase to double the sound pressure and a 10-dB increase to double the psychoacoustic loudness (Schomer, 1978), the 32.0-dB difference in peak SPLs observed between the MB-SWIFT and EPI indicates a 39.8 times higher peak sound pressure and a 9.2 times higher peak loudness during EPI compared with MB-SWIFT. Regarding the average SPLs, the 8-slice EPI (8.4 dB higher compared with MB-SWIFT) and 15-slice EPI (19.7 dB higher compared with MB-SWIFT) sequences had 2.6 and 9.7 times higher average SPLs, and were 1.8 and 3.9 times louder than MB-SWIFT, respectively.

The representative spectrograms in Fig. 1B suggest that the MB-SWIFT-induced sound mainly consists of frequencies up to 15 kHz, while intense frequencies throughout the measurement range (up to 22 kHz) are present during the SE-EPI sequence. This is important as rats have the highest auditory sensitivity around 12–24 kHz (Borg, 1982), which clearly differs from the 2–5 kHz range in humans.

Representative audio samples are available in the supplementary material. The recording gain was same across the samples, allowing for direct comparison of the audible loudness across the files.

3.2. The effect of body movement on fMRI

The effect of controlled body movements on SE-EPI and MB-SWIFT fMRI data is summarized in Fig. 2, and a representative dataset showing the body movement-induced B_0 frequency shifts is shown in Supplementary Fig. 1. Motion correction was not used at this stage, as the skull was tightly fixed and did not move physically during the experiments. During SE-EPI, body movement had a significant and widespread influence on voxels throughout the FOV (Fig. 2A). The statistical maps suggest a ventral shift and/or squeeze of roughly two voxels in each experiment, as the red-yellow clusters (Fig. 2A) form the shape of the head below the position of the head in the baseline image. Analysis of images across time confirmed that the brain is apparently moving down (~2–3 mm) in the phase encoding (vertical) direction. In contrast, a minimal number of voxels was affected during the MB-SWIFT sequence, which most likely originates from the insensitivity of MB-SWIFT to the B_0 shifts. The few apparently activated voxels in MB-SWIFT images were mainly on the skin outside the brain. Prior to the experiments, it was observed that the skin around the head was stretching because of the body movement, which is consistent with the ostensibly activated voxels with MB-SWIFT. The average time-series obtained from the cortex (Fig. 2B) confirms that the body movement did not affect the MB-SWIFT

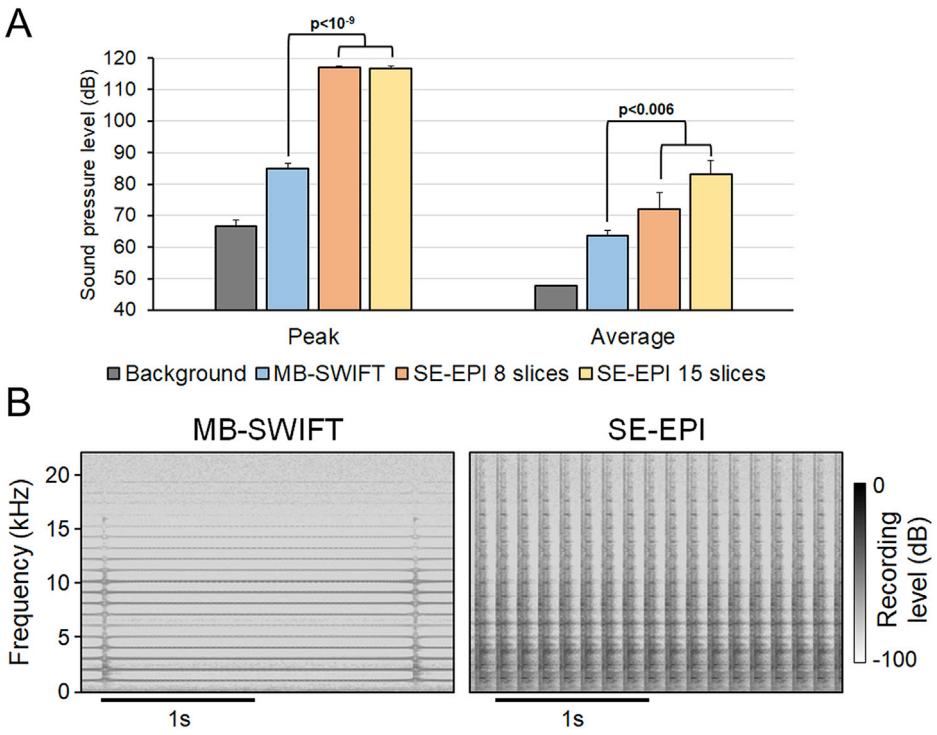

Fig. 1. Peak and average sound pressure levels (A), and representative sound spectrograms (B) measured inside the 9.4T MRI bore during MB-SWIFT and SE-EPI. Measurements were repeated 5–10 times per condition. Values in panel A are mean ± SD. The SE-EPI sequence in panel B includes 15 slices within a repetition time of 2 s. The statistics shown in panel A were calculated using a two-tailed Student's *t*-test.

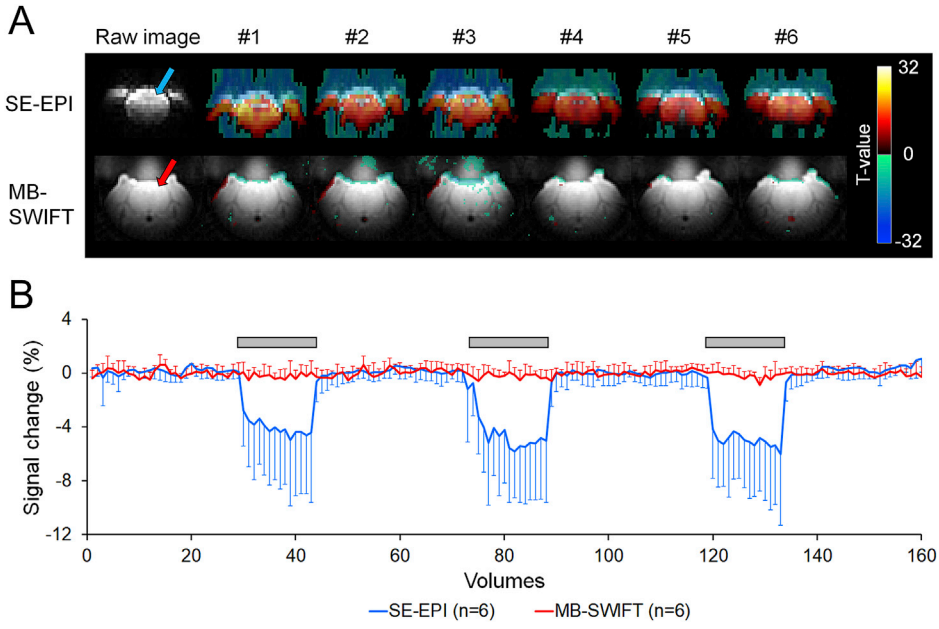

Fig. 2. Effect of controlled body movement on fMRI images (A) and signal intensity (B). Motion correction was not used at this stage. On the left of the panel A, unprocessed single slice fMRI images acquired with SE-EPI or MB-SWIFT sequences are shown. Statistical activation maps (block-model design general linear model, $p < 0.001$, false discovery rate corrected) obtained from each individual experiment (#1-#6) are shown next to the raw images. Representative group-averaged fMRI time series obtained from the cortex are shown in panel B. Blue and red arrows in raw images in panel A indicate the regions from which the time series were obtained. The gray bars in panel B indicate the time periods of controlled body movement. The values in panel B are mean ± SD.

fMRI signal, while the signal variation was considerable during SE-EPI.

Because SE-EPI images were heavily affected by the body movement, the SE-EPI data were motion-corrected and compared to uncorrected SE-EPI data to investigate whether motion correction would improve the data quality. The motion correction parameters closely followed the changes observed in voxel-level time series, which confirms that apparent motion explains the majority of the signal changes. The group-level time-series revealed that rigid ANTs motion correction fails to correct the movement-induced signal losses and blurring observed with the SE-EPI sequence (Supplementary Fig. 2). When affine ANTs were used and combined with the regression of the obtained 12 motion correction parameters, the group-level time-series improved considerably (Supplementary Fig. 2). The statistical tests, however, indicated that 2 of the 6 datasets were still affected by movement.

Due to the minimal influence of body movement on MB-SWIFT images, we tested whether the MB-SWIFT data quality in the body movement experiment was good enough to allow for resting-state analyses. The group-level ICA revealed a clear network (Fig. 3) commonly observed in isoflurane-anesthetized rats related to the cortical burst-suppression activity (Liu et al., 2011; Paasonen et al., 2018),

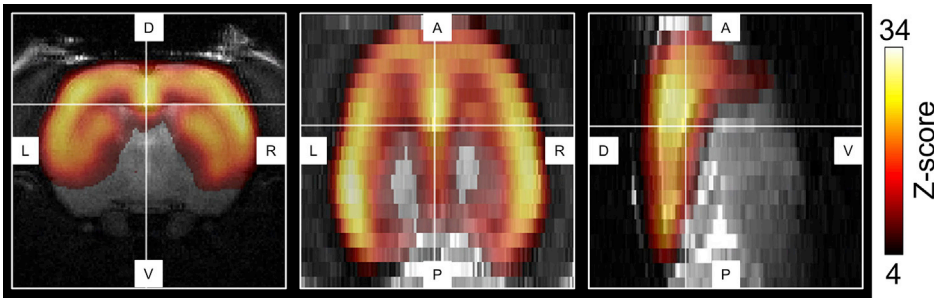

Fig. 3. Group-level independent component representing the isoflurane-induced cortical burst suppression activity, measured during the controlled body movement experiment with MB-SWIFT in anesthetized rats. The statistical map is overlaid on an anatomical T_2-weighted image. No motion correction or brain masking was applied. All MB-SWIFT fMRI data shown in Fig. 2 were included in the independent component analysis. A, anterior; D, dorsal; L, left; P, posterior; R, right; V, ventral.

suggesting that even a significant body movement during MB-SWIFT fMRI may not prevent the identification of functional networks. With SE-EPI data, controlled body movement accounted for the vast majority of the variance in ICA, and the corresponding component was not visible with either rigid or affine corrections including the regression of motion parameters (data not shown).

A video showing the actual body movement during the experiments is available in the supplementary material.

Supplementary video related to this article can be found at https://doi.org/10.1016/j.neuroimage.2019.116338.

3.3. Awake rat functional connectivity measurements with MB-SWIFT

The movement of animals during MB-SWIFT (0.48 ± 0.23 events/

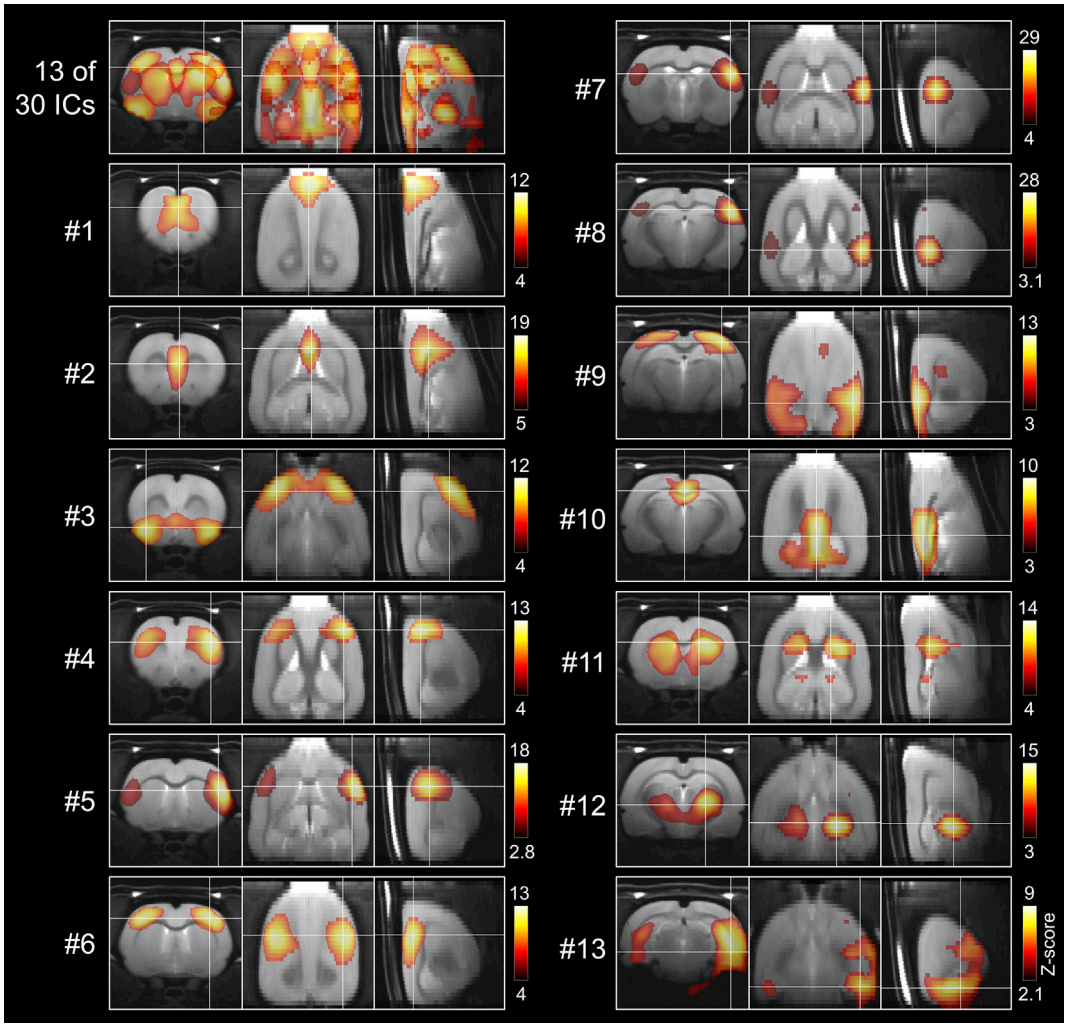

Fig. 4. Anatomically well-defined group-level independent components obtained with MB-SWIFT and independent component analysis from awake rats. The data-driven analysis was set to run with 30 components, of which 13 anatomically best localized bilateral components are shown. On top left, all 13 selected components are shown together, while the rest of the figure represents each component individually. The components are numbered from anterior cortical components to posterior subcortical components. The statistical maps are overlaid on anatomical T_2-weighted images. The orientation of images is same as in Fig. 3. IC, independent component.

min) was less frequent ($p = 0.03$, two-tailed Student's *t*-test) than in our previous awake SE-EPI experiments (1.00 ± 0.58 events/min) (Stenroos et al., 2018). Out of 750 measured volumes, 658 ± 92 (87.7%) volumes per rat were included into the ICA analysis after excluding data periods affected by movement. Both parameters indicate that the measurements were successful.

The group-level awake rat ICA results summarized in Fig. 4 show that MB-SWIFT fMRI can be used to parcellate brain resting-state activity in an awake rat at an excellent spatial level. Multiple anatomically well-localized bilateral components were identified, suggesting distinct functionally connected networks. The cortical connectivity was divided into several components, including the anterior frontal (#1), medial frontal (#2), orbital frontal (#3), motor (#4), insular (#5), somatosensory (#6), auditory (#7–8), visual (#9), and retrosplenial (#10) cortices. For both striatum and thalamus well-localized components were observed (#11 and #12, respectively). The hippocampal component, however, was somewhat vague and limited to the temporal (ventral) part. Nevertheless, the observed components covered most of the cortical regions, large parts of striatum and thalamus, and some parts of hippocampus, leading to almost whole brain level functional segregation.

The correlation matrices (Fig. 5) showed strong correlation (0.6–0.7) patterns between several cortical ICs, which formed clear clusters of high correlations. This suggests that these specific components inside the squares form subnetworks or modules, such as prefrontal, lateral frontal, and parietal cortical networks, where more intensive FC is expressed within the network. Additionally, the striatal component (#11) consistently correlated with several cortical components (#1–6), indicating robust subcortico-cortical activity. The standard deviations are shown in Supplementary Fig. 3.

3.4. Simultaneous EEG and MB-SWIFT fMRI

From one dataset out of six (10 min each), the last 3 min of EEG data were discarded due to signal artefacts originating from external noise.

The investigation of MRI-induced EEG artefacts (Fig. 6A) indicates that the SE-EPI-induced artefacts (16 ± 6.5 mV) are roughly an order of magnitude higher in amplitude than those induced by MB-SWIFT (1.7 ± 0.4 mV; $p = 0.02$, Student's *t*-test, one representative artefact per rat). The periodic low amplitude artefacts observed during MB-SWIFT (Fig. 6B, top row) can be effectively removed with standard artefact-removal approaches (Fig. 6B, bottom row).

Fig. 6C shows that compared with SE-EPI, MB-SWIFT is rather insensitive to image distortions induced by the surgical operations and EEG electrodes. Compared with the FSEMS image, the SE-EPI image shows vertical stretching of the cortex in regions close to the measuring electrodes (white arrows). Additionally, the lateral parts of the cortex in the same image show signal pile-up artefacts (red arrows), observed as cortical thinning. Additionally, the air cavities disturb the brain shape in the SE-EPI image in the lower brain regions (yellow arrows). No similar artefacts are observed in MB-SWIFT images. Thus, it appears that while using MB-SWIFT in simultaneous EEG measurements, the whole brain, including regions close to the measuring electrodes, can be analyzed.

To demonstrate this, Fig. 7A shows representative data where the correspondence between the HRF-convolved EEG envelope and MB-

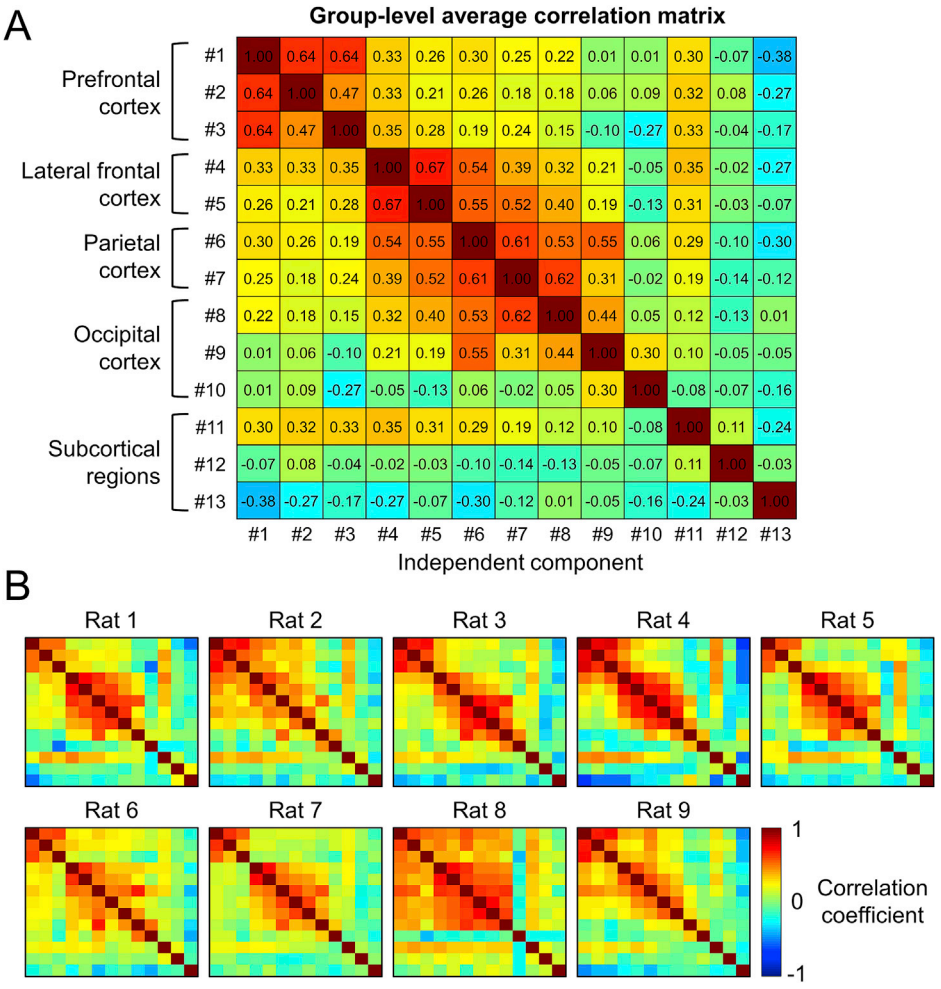

Fig. 5. Group-level (A) and individual-level (B) correlation matrices obtained between independent components of awake rats. The numbering of independent components corresponds to that in Fig. 4.

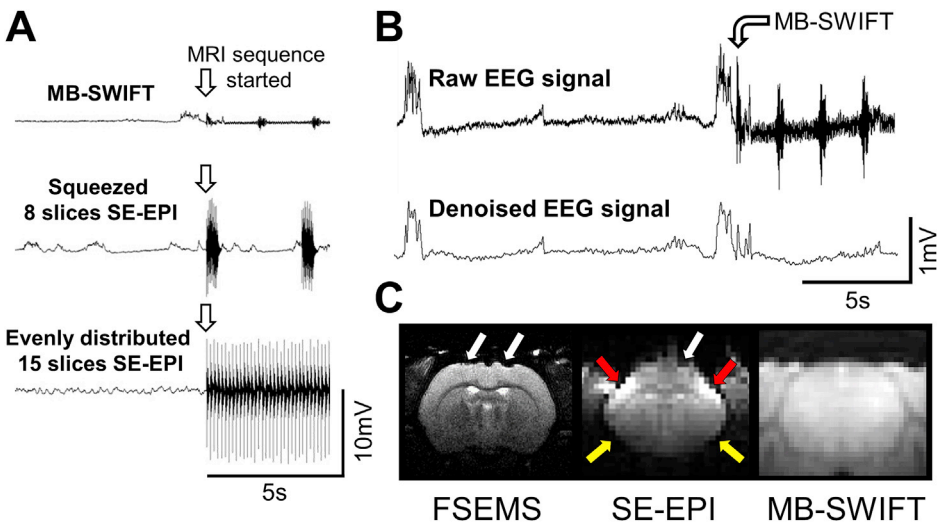

Fig. 6. Examples of the fMRI gradient switching artefact amplitudes in EEG signals (A), raw and denoised EEG signals obtained during EEG/MB-SWIFT fMRI (B), and EEG-electrode-induced image distortions (C) during simultaneous EEG-fMRI in an isoflurane-anesthetized rat. Panel A shows that the gradient artefacts are roughly 10 times higher during SE-EPI compared with MB-SWIFT (15 mV and 1.5 mV, respectively). The voltage scale is the same for all three EEG signals in section A, while a smaller voltage scale is used for the two signals in section B. The white arrows in panel C indicate the electrode-induced signal distortions in fast spin echo multi slice (FSEMS) and spin echo echo planar imaging (SE-EPI) images. Red arrows indicate signal pile-up artefacts in SE-EPI images. Yellow arrows show typical distortions in the lower brain regions around air cavities in SE-EPI fMRI images. Compared with FSEMS and SE-EPI images, no distortions were observed in MB-SWIFT images.

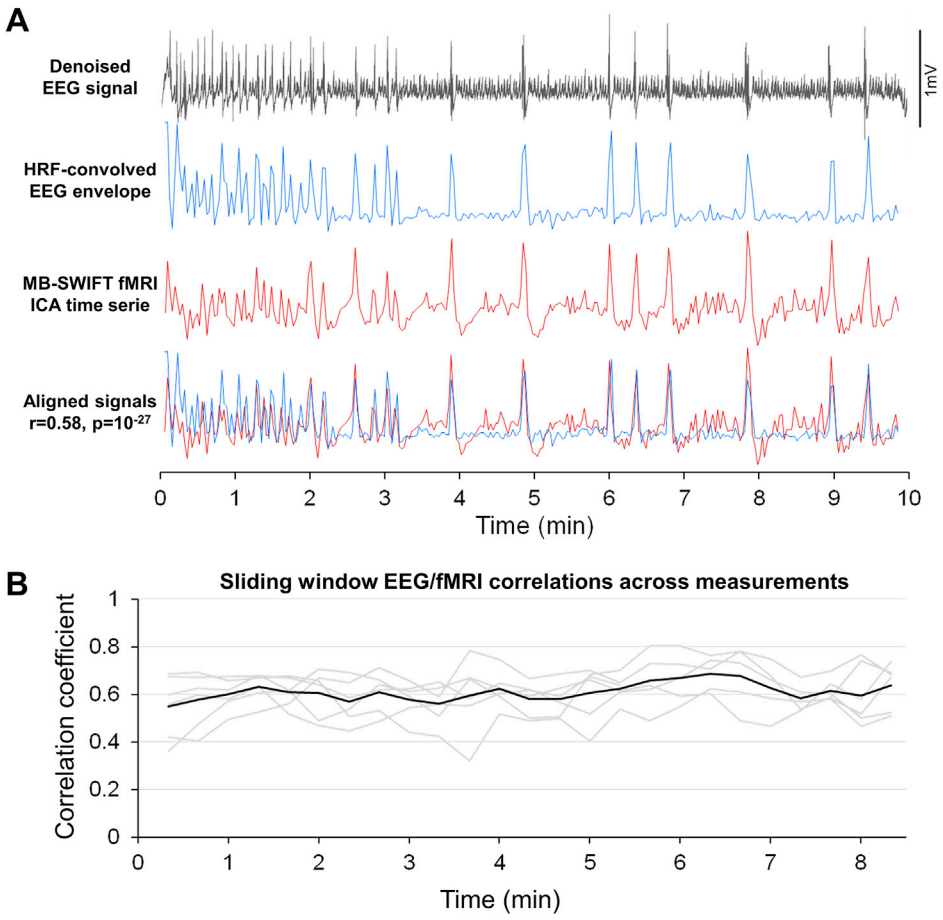

Fig. 7. Representative simultaneous EEG-fMRI data obtained from one isoflurane-anesthetized rat (A), and temporal partial sliding window correlations between EEG and fMRI signals across all measurements (B). EEG was measured from the somatosensory cortex. The denoised EEG signal envelope was convolved with a hemodynamic response function (HRF) of a rat and compared with the cortical component of the MB-SWIFT signal obtained with independent component analysis (ICA; component corresponding to the one shown in Fig. 3). Sliding window analysis (50 vol windows with 10 vol steps) estimates the temporal stability of the correlation between EEG and MB-SWIFT fMRI signals (B). Black line in B represents the average across measurements (gray lines). Three rats were imaged, each having two cortical electrodes. EEG, electroencephalography; HRF, hemodynamic response function; ICA, independent component analysis.

SWIFT fMRI signal during moderate isoflurane-induced burst-suppression activity is very clear. Cortical bursts were well aligned between signals during both fast (first 3 min) and slow (from 4 to 10 min) bursting patterns. The group-level average correlation between measured EEG signals ($n = 6$) and cortical hemodynamic MB-SWIFT components was 0.57 ± 0.04 (in all cases $p < 10^{-16}$).

As the depth of anesthesia, and thus the burst-suppression pattern and incidence, varied slightly during the measurements and across animals, the temporal stability and condition-dependency of the EEG/MB-SWIFT fMRI correlations was investigated with a sliding window analysis. Despite the varying neuronal activity, a very stable correlation of around 0.6 was observed between neuronal activity and fMRI signal throughout the measurements and subjects (Fig. 7B), indicating the robustness of the method.

4. Discussion

In the present study, MB-SWIFT was used for the first time in FC

studies, in awake rat experiments, and in simultaneous electrophysiological and fMRI measurements. The results indicate that MB-SWIFT is a robust functional brain mapping tool that can overcome many of the limitations associated with conventional EPI fMRI at high magnetic fields.

4.1. Acoustic scanner noise during fMRI

Acoustic scanner noise is a serious issue in fMRI, as it can induce hearing loss and stress (Lauer et al., 2012) and confound the fMRI results in both stimulus evoked and resting-state applications by direct and/or indirect mechanisms (Moelker and Pattynama, 2003). As the trend in fMRI has constantly been towards higher spatial and temporal resolution in higher magnetic fields, there is an urgent need for alternative options to loud EPI sequences, especially for awake imaging. To achieve close to isotropic resolution with a traditional 2D EPI sequence, the slice number has to be quite high. In the current study, an increase from 8 to 15 slices (TR = 2 s) in SE-EPI almost quadruples the average SPL (+11.3 dB). In many studies, same number of slices is squeezed within TR = 1 s, which drastically increases SPLs. Additionally, the Lorentz forces behind the acoustic noises increase logarithmically with the main magnetic field and the gradient currents (Mansfield et al., 1998), inducing more pronounced scanner noise in ultra-high fields with small voxels.

Although comparative animal studies are limited, recent human studies indicate that the use of more silent fMRI sequences, such as EPI with a sinusoidal readout gradient and interleaved silent steady state, significantly improves the data quality, e.g., in working memory tasks (Tomasi et al., 2005), auditory stimuli experiments (Schmitter et al., 2008), and FC measurements (Andoh et al., 2017). In these studies, the "silent" sequences were 7.2–20 dB quieter than the standard fMRI sequence of the group. Here, MB-SWIFT was found to have a roughly 32-dB and 20-dB lower peak and average SPL, respectively, compared with our standard fMRI sequence. This is a major improvement, as for both rat and human, the loudness grows as described by Steven's law (Pierrel-Sorrentino and Raslear, 1980), and thus lower SPL can be considered more comfortable for both species. Indeed, the degree of animal movement during the awake rat MB-SWIFT fMRI experiments was only half of that observed during SE-EPI fMRI in our previous study (Stenroos et al., 2018), in which a similar training protocol and lower 7 T field were used. The reduced movement supports the choice of more silent sequences in awake animal studies, as a significant reduction in movement directly enhances data quality. In addition, such data possibly reflect more stress-free and normal brain function without confounding acoustic stimulus-induced modulation. We have, however, no direct biological measures to confirm decreased stress levels during MB-SWIFT in the current study.

Although discussion related to acoustic scanner noise is typically focused on SPLs, there are other important factors to consider. A recent study reported a clear difference in the resting-state network characteristics between continuous and periodical data acquisition approaches, where periodical scanning is considered to have more disturbing effects on FC (Langers and van Dijk, 2011). This might be especially important in certain EPI studies, where a long TR is used to allow for the acquisition of a clean electrophysiological signal between fMRI images. From this viewpoint, MB-SWIFT is a particularly advantageous sequence because it allows for continuous data acquisition and relatively stable SPL with no audible pauses.

Additionally, auditory sensitivity differs across species. Compared with humans, the auditory sensitivity of rats is shifted to higher frequencies, as the highest sensitivity begins around 8–12 kHz and extends up to 38 kHz (Borg, 1982; Kelly and Masterton, 1977). In mice the highest sensitivity starts around 15 kHz (Lauer et al., 2012). Interestingly, the MB-SWIFT-induced scanner noise appears to contribute only minimally to frequencies higher than 12 kHz, while during SE-EPI frequencies up to 22 kHz and likely beyond are present (Fig. 1B). Therefore, besides lower SPL induced by MB-SWIFT, the acoustic frequency spectrum, which avoids the highest auditory sensitivity of rat, may improve the quality of the data obtained in awake rats.

As the main auditory sensitivity of rats extends up to 38 kHz, the lack of ultrasound coverage is a shortcoming in our acoustic measurements. Frequencies higher than 22 kHz, however, are aliased into the measured signal and likely contribute to the total SPL, making comparison between the sequences reasonable.

4.2. Dynamic movement-induced local field fluctuations during fMRI

Subject movement during fMRI is a major concern, as up to 90% of the signal variance may be explained by motion (Friston et al., 1996). In general, three types of movement occur during MRI: periodic involuntary movements (e.g., respiration-induced chest and lung cavity movement), sudden involuntary movements (e.g., swallowing and eye blinking), and conscious body part movements (Godenschweger et al., 2016).

Even if the movement does not occur physically inside the FOV, as in our controlled body movement experiment, it induces changes in B_0-field that can extend and induce local field offsets inside the FOV. For example, in EPI fMRI, the respiratory cycle explains a major part of the physiological noise in humans (Bianciardi et al., 2014), and is tightly coupled with the phase encoding voxel shifts in rats (Kalthoff et al., 2011). EPI is particularly sensitive to any local field offsets in the phase encoding direction due to its low bandwidth, and is thus prone to spatial voxel shifts, image distortions, and signal drops (Jezzard, 2012).

Several modern approaches have been developed to correct for the motion artefacts occurring during EPI fMRI, yet none is able to fully recover the data (Zaitsev et al., 2017). Additionally, the constant shift towards ultra-high fields complicates shimming, and is likely to emphasize the field inhomogeneity and motion artefact issues in EPI as they are field-dependent (Jezzard, 2012; Raj et al., 2000).

Although the SE-EPI images were affected by body movement in our study, they induced only minor to no effects on MB-SWIFT images. This is due to the high acquisition bandwidth of MB-SWIFT in all spatial encoding directions so that dynamic local field offsets are not high enough to deform the image or shift voxels. The temporary body relocation in our controlled movement experiments was estimated to exceed the scale of normal involuntary movements, such as breathing and muscle twitching, and to be in a similar range as conscious movements. Hence, MB-SWIFT is rather insensitive to movement-induced artefacts originating from outside the FOV. Movement occurring inside the FOV is still problematic, although radial sampling offers better resilience to movement as the center of the k-space is typically oversampled compared with Cartesian sampling (Glover and Pauly, 1992).

4.3. Brain functional connectivity in awake rats measured with MB-SWIFT

There is a growing interest in awake rodent fMRI imaging (King et al., 2005; Lahti et al., 1998) to allow for behavioral study settings and thus increased translational value of the preclinical experiments. Early awake rat FC studies demonstrated anatomically well-localized signal fluctuations between several brain regions important for emotional and cognitive functions (Zhang et al., 2010). Later it was demonstrated that such fluctuations are confounded by anesthetics (Liang et al., 2015; Paasonen et al., 2018; Smith et al., 2017). Despite the clear advantages of awake rat imaging, subject motion and stress remain among the biggest hurdles (King et al., 2005).

Comparing the exact amount of movement artefacts during awake rat fMRI studies across laboratories is difficult, as there are no established convergent methods to analyze or report these artefacts. Nevertheless, compared with our previous SE-EPI studies (Stenroos et al., 2018), the number of movements during MB-SWIFT was significantly smaller, most likely because of a different type of acoustic scanner noise, as discussed earlier. This can be considered a significant methodological improvement.

The fMRI FC studies conducted so far in awake rats have exploited

EPI, which raises concern over whether the FC data obtained with MB-SWIFT and those obtained with the current gold standard are comparable. To allow for comparison as generalizable as possible, simple and straightforward data-driven analyses were used to estimate FC in the current study. In general, our FC results obtained with MB-SWIFT are in excellent agreement with those obtained in previous EPI studies (Becerra et al., 2011; Liang et al., 2011; Liang et al., 2015; Ma et al., 2018; Paasonen et al., 2018; Smith et al., 2017; Zhang et al., 2010).

Zhang et al. (2010) and Liang et al. (2015) reported a moderate correlation between prefrontal cortex and parietal cortex, and retrosplenial cortex and visual cortex, similar to our results. The ICs reported by Liang et al. (2011) appear to be very close to the components shown in Fig. 4, with small differences likely originating from our stricter component exclusion criteria. Becerra et al. (2011) showed cortical and thalamic ICs similar to our results. Moderate correlations between the striatum and prefrontal cortex, and between the insular and parietal cortices were reported by Smith et al. (2017), and match our results. The low-dimensionality functional atlas suggested by Ma et al. (2018) largely resembles our functional parcellation. Lastly, we previously reported moderate to good correlations across cortical regions, between the striatum and cortical regions, and between the prefrontal cortex and parietal cortex (Paasonen et al., 2018), which also support our current findings.

Although a default mode network is reported to exist in anesthetized rats (Lu et al., 2012), the awake rat studies to date have yielded no clear and convergent results. The spatial maps of putative default mode-like activity in early awake rat reports by (Upadhyay et al., 2011) and Zhang et al. (2010) overlap only partially with the maps obtained in anesthetized rats (Lu et al., 2012). Similarly, the current work did not detect ICs corresponding specifically to the default mode network reported by Lu et al. (2012). Instead, several ICs overlapping parts of the suggested rat default mode network were observed, including medial frontal, anterior cingulate, retrosplenial, and parietal cortices. The reason for the discrepancy between the above-mentioned observations can only be speculated, but as the animals are still in an unnatural environment, one explanation could be a de-activation of the default mode due to sensory and cognitive processing. Therefore, more thorough investigations are required to properly define the default mode network in awake rats (Becerra et al., 2011).

Taken together, the FC data obtained with MB-SWIFT in awake rats are consistent with those obtained in previous EPI studies. Despite the relatively small number of subjects (n = 9), the data-driven ICA was able to achieve near whole-brain functional parcellation, which has not been routinely achieved with even larger group sizes (typical n = 15–42) in previous awake rat EPI studies.

4.4. Simultaneous EEG and fMRI measurements with MB-SWIFT

Simultaneous EEG and fMRI measurements provide a combination of millisecond resolution and whole-brain coverage, respectively, but also combined information related to the electrical, vascular, and metabolic activity of the brain (Mirsattari et al., 2007; Pirttimaki et al., 2016). Despite the clear advantage of concurrent measurements, recordings are often performed separately due to technical challenges.

In the current study, we show that neither silver wire electrodes on the dura nor the surgical procedures influence MB-SWIFT images, whereas they induce clear distortions in SE-EPI images. Our previous study showed that a deep brain electrode made of tungsten wire induces only minimal image distortions in MB-SWIFT compared with SE-EPI (Lehto et al., 2017). It is worth mentioning that the image distortions are even more severe in commonly used gradient echo EPI. Distortion-free MB-SWIFT images not only allow for analysis of regions immediately next to the electrodes, but also regions next to air cavities, such as the amygdala. The insensitivity to susceptibility-induced deformations and signal voids originates from the large acquisition bandwidth and zero acquisition delay of MB-SWIFT.

The main MRI-induced artefact in EEG is the gradient switching-induced current, which can heavily mask the biological EEG signal (Mirsattari et al., 2007). While the electrophysiological signal typically varies in the scale of 0.5 mV, EPI-induced currents can range from 5 mV up to more than 20 mV (Pan et al., 2011; Sumiyoshi et al., 2011), which fits well with our current findings (Fig. 6A). Modern real-time and/or post-processing protocols are able to remove the EPI-induced artefacts almost completely (Mirsattari et al., 2005; Pan et al., 2011), but only if the amplifier is not saturated by the MRI artefact. Saturated signal cannot be recovered, and it can take hundreds of milliseconds for the signal to again reach a steady state. Hence, the significantly lower currents in EEG induced by MB-SWIFT provide a safer approach for simultaneous EEG-fMRI under suboptimal experimental conditions.

In the present work, there was a clear correspondence between electrical activity and the HRF-convolved MB-SWIFT time-course in the isoflurane-anesthetized rats. The results in Fig. 7 closely resemble the findings characterizing the coupling between EEG and cerebral blood flow under isoflurane-induced burst-suppression activity (Liu et al., 2011). Liu et al. (2011) reported correlation values ~0.6 between laser Doppler-measured blood flow and EEG, while another study reported slightly lower correlation values (~0.4) between BOLD and local field potentials (Pan et al., 2011). Thus, it appears that MB-SWIFT indirectly follows the neuronal activity at least as well as laser Doppler flowmetry and EPI fMRI in isoflurane-anesthetized rats.

Simultaneous EEG/SE-EPI data acquired in the current work was not analyzed, as the cortical regions were considered to be heavily distorted (Fig. 6C). The surgical procedures were slightly different from those in our previous report, in which chronic electrodes were implanted for measurements at 7 T (Pirttimaki et al., 2016). Thus, the EPI distortions in the current study likely originate from the higher magnetic field, and from the open interface between the air and skull. Nevertheless, these observations emphasize the insensitivity of MB-SWIFT to susceptibility-induced artefacts in complex experimental protocols.

4.5. Limitations of MB-SWIFT

Because MB-SWIFT has a near zero echo time and no volume selection, there are some methodological limitations. First, signal is received from everything that includes protons with a T_2 of tens of microseconds and longer and is in the range of the transmitter/receiver coils. As it is practically very challenging to have all materials in the setup free of protons, the FOV has to cover everything that the receiver coil typically sees.

Second, because the MB-SWIFT fMRI images have a low anatomical contrast, standard motion correction and co-registration methods fail to register the images correctly. In addition to signal intensity correction, motion correction and co-registration require adjustments to algorithm parameters or the use of indirect methods.

Third, as any pulse using high excitation bandwidth, MB-SWIFT can become a high-SAR pulse sequence. We estimated the rat head SAR to be approximately 20 W/kg at 9.4 T, which translates to approximately 2 W/kg at 3 T (Lehto et al., 2017). As this is below, e.g., the FDA head SAR limit (https://www.aapm.org/meetings/02AM/pdf/8356-48054.pdf), MB-SWIFT fMRI using such high excitation bandwidth, flip angle, and time resolution is also feasible in humans.

5. Conclusions

Our results demonstrate that MB-SWIFT has unique features that make it a valuable tool for preclinical fMRI studies. The 20-dB difference in the average SPL between the MB-SWIFT technique and our standard EPI pulse sequence clearly exceeds the typical drop of 12 dB with silent EPI pulse sequences (Hutter et al., 2018; Zapp et al., 2012). In addition to the low acoustic noise, the insensitivity to movement and susceptibility-induced artefacts make MB-SWIFT ideal for awake rodent studies and simultaneous EEG-fMRI measurements. Importantly, the

fMRI results were of high quality and consistent with those of previous EPI studies, indicating that MB-SWIFT is a valid alternative to EPI for demanding fMRI protocols. The benefits of MB-SWIFT enable fMRI study designs involving complex experimental setups at high magnetic fields.

Acknowledgements

We thank Mikko Nissi, PhD, and Olli Nykänen, MSc, for technical assistance in the field map experiments. This work was supported by the National Institutes of Health (U01-NS103569 and P41-EB015894); Academy of Finland (#298007); and the Jane and Aatos Erkko Foundation. The authors have no conflicts of interest to disclose.

Appendix A. Supplementary data

Supplementary data to this article can be found online at https://doi.org/10.1016/j.neuroimage.2019.116338.

References

Andoh, J., Ferreira, M., Leppert, I.R., Matsushita, R., Pike, B., Zatorre, R.J., 2017. How restful is it with all that noise? comparison of interleaved silent steady state (ISSS) and conventional imaging in resting-state fMRI. Neuroimage 147, 726–735.
Avants, B.B., Tustison, N.J., Song, G., Cook, P.A., Klein, A., Gee, J.C., 2011. A reproducible evaluation of ANTs similarity metric performance in brain image registration. Neuroimage 54 (3), 2033–2044.
Becerra, L., Pendse, G., Chang, P.C., Bishop, J., Borsook, D., 2011. Robust reproducible resting state networks in the awake rodent brain. PLoS One 6 (10), e25701.
Beck, A., Teboulle, M., 2009. Fast gradient-based algorithms for constrained total variation image denoising and deblurring problems. IEEE Trans. Image Process. Public. IEEE Signal Process. Soc. 18 (11), 2419–2434.
Bianciardi, M., van Gelderen, P., Duyn, J.H., 2014. Investigation of BOLD fMRI resonance frequency shifts and quantitative susceptibility changes at 7 T. Hum. Brain Mapp. 35 (5), 2191–2205.
Borg, E., 1982. Auditory thresholds in rats of different age and strain. A behavioral and electrophysiological study. Hear. Res. 8 (2), 101–115.
Friston, K.J., Williams, S., Howard, R., Frackowiak, R.S., Turner, R., 1996. Movement-related effects in fMRI time-series. Magn. Reson. Med. 35 (3), 346–355.
Glover, G.H., Pauly, J.M., 1992. Projection reconstruction techniques for reduction of motion effects in MRI. Magn. Reson. Med. 28 (2), 275–289.
Godenschweger, F., Kagebein, U., Stucht, D., Yarach, U., Sciarra, A., Yakupov, R., Lusebrink, F., Schulze, P., Speck, O., 2016. Motion correction in MRI of the brain. Phys. Med. Biol. 61 (5), R32–R56.
Grandjean, J., Schroeter, A., Batata, I., Rudin, M., 2014. Optimization of anesthesia protocol for resting-state fMRI in mice based on differential effects of anesthetics on functional connectivity patterns. Neuroimage 102 (Pt 2), 838–847.
Hutter, J., Price, A.N., Cordero-Grande, L., Malik, S., Ferrazzi, G., Gaspar, A., Hughes, E.J., Christiaens, D., McCabe, L., Schneider, T., others, 2018. Quiet echo planar imaging for functional and diffusion MRI. Magn. Reson. Med. 79 (3), 1447–1459.
Huttunen, J.K., Grohn, O., Penttonen, M., 2008. Coupling between simultaneously recorded BOLD response and neuronal activity in the rat somatosensory cortex. Neuroimage 39 (2), 775–785.
Idiyatullin, D., Corum, C.A., Garwood, M., 2015. Multi-band-SWIFT. J. Magn. Reson. 251, 19–25.
Idiyatullin, D., Corum, C., Park, J.Y., Garwood, M., 2006. Fast and quiet MRI using a swept radiofrequency. J. Magn. Reson. 181 (2), 342–349.
In, M.H., Cho, S., Shu, Y., Min, H.K., Bernstein, M.A., Speck, O., Lee, K.H., Jo, H.J., 2017. Correction of metal-induced susceptibility artifacts for functional MRI during deep brain stimulation. Neuroimage 158, 26–36.
Jezzard, P., 2012. Correction of geometric distortion in fMRI data. Neuroimage 62 (2), 648–651.
Jonckers, E., Delgado y Palacios, R., Shah, D., Guglielmetti, C., Verhoye, M., Van der Linden, A., 2014. Different anesthesia regimes modulate the functional connectivity outcome in mice. Magn. Reson. Med. 72 (4), 1103–1112.
Kalthoff, D., JU, Seehafer, Po, C., Wiedermann, D., Hoehn, M., 2011. Functional connectivity in the rat at 11.7T: impact of physiological noise in resting state fMRI. Neuroimage 54 (4), 2828–2839.
Kelly, J.B., Masterton, B., 1977. Auditory sensitivity of the albino rat. J. Comp. Physiol. Psychol. 91 (4), 930–936.
King, J.A., Garelick, T.S., Brevard, M.E., Chen, W., Messenger, T.L., Duong, T.Q., Ferris, C.F., 2005. Procedure for minimizing stress for fMRI studies in conscious rats. J. Neurosci. Methods 148 (2), 154–160.
Lahti, K.M., Ferris, C.F., Li, F., Sotak, C.H., King, J.A., 1998. Imaging brain activity in conscious animals using functional MRI. J. Neurosci. Methods 82 (1), 75–83.
Langers, D.R., van Dijk, P., 2011. Robustness of intrinsic connectivity networks in the human brain to the presence of acoustic scanner noise. Neuroimage 55 (4), 1617–1632.
Lauer, A.M., El-Sharkawy, A.M., Kraitchman, D.L., Edelstein, W.A., 2012. MRI acoustic noise can harm experimental and companion animals. J. Magn. Reson. Imaging JMRI 36 (3), 743–747.
Lehto, L.J., Idiyatullin, D., Zhang, J., Utecht, L., Adriany, G., Garwood, M., Grohn, O., Michaeli, S., Mangia, S., 2017. MB-SWIFT functional MRI during deep brain stimulation in rats. Neuroimage 159, 443–448.
Liang, Z., Liu, X., Zhang, N., 2015. Dynamic resting state functional connectivity in awake and anesthetized rodents. Neuroimage 104, 89–99.
Liang, Z., King, J., Zhang, N., 2011. Uncovering intrinsic connectional architecture of functional networks in awake rat brain. J. Neurosci. Off. J. Soc. Neurosci. 31 (10), 3776–3783.
Liu, X., Zhu, X.H., Zhang, Y., Chen, W., 2011. Neural origin of spontaneous hemodynamic fluctuations in rats under burst-suppression anesthesia condition. Cerebr. Cortex 21 (2), 374–384.
Lu, H., Zou, Q., Gu, H., Raichle, M.E., Stein, E.A., Yang, Y., 2012. Rat brains also have a default mode network. Proc. Natl. Acad. Sci. U. S. A 109 (10), 3979–3984.
Lukasik, V.M., Gillies, R.J., 2003. Animal anaesthesia for in vivo magnetic resonance. NMR Biomed. 16 (8), 459–467.
Ma, Z., Perez, P., Ma, Z., Liu, Y., Hamilton, C., Liang, Z., Zhang, N., 2018. Functional atlas of the awake rat brain: a neuroimaging study of rat brain specialization and integration. Neuroimage 170, 95–112.
Mansfield, P., Glover, P.M., Beaumont, J., 1998. Sound generation in gradient coil structures for MRI. Magn. Reson. Med. 39 (4), 539–550.
Mirsattari, S.M., Ives, J.R., Leung, L.S., Menon, R.S., 2007. EEG monitoring during functional MRI in animal models. Epilepsia 48 (Suppl. 4), 37–46.
Mirsattari, S.M., Ives, J.R., Bihari, F., Leung, L.S., Menon, R.S., Bartha, R., 2005. Real-time display of artifact-free electroencephalography during functional magnetic resonance imaging and magnetic resonance spectroscopy in an animal model of epilepsy. Magn. Reson. Med. 53 (2), 456–464.
Moelker, A., Pattynama, P.M., 2003. Acoustic noise concerns in functional magnetic resonance imaging. Hum. Brain Mapp. 20 (3), 123–141.
Moeller, S., Yacoub, E., Olman, C.A., Auerbach, E., Strupp, J., Harel, N., Ugurbil, K., 2010. Multiband multislice GE-EPI at 7 tesla, with 16-fold acceleration using partial parallel imaging with application to high spatial and temporal whole-brain fMRI. Magn. Reson. Med. 63 (5), 1144–1153.
Ogawa, S., Lee, T.M., Kay, A.R., Tank, D.W., 1990. Brain magnetic resonance imaging with contrast dependent on blood oxygenation. Proc. Natl. Acad. Sci. U. S. A 87 (24), 9868–9872.
Paasonen, J., Salo, R.A., Huttunen, J.K., Grohn, O., 2017. Resting-state functional MRI as a tool for evaluating brain hemodynamic responsiveness to external stimuli in rats. Magn. Reson. Med. 78 (3), 1136–1146.
Paasonen, J., Stenroos, P., Salo, R.A., Kiviniemi, V., Grohn, O., 2018. Functional connectivity under six anesthesia protocols and the awake condition in rat brain. Neuroimage 172, 9–20.
Paasonen, J., Salo, R.A., Shatillo, A., Forsberg, M.M., Narvainen, J., Huttunen, J.K., Grohn, O., 2016. Comparison of seven different anesthesia protocols for nicotine pharmacologic magnetic resonance imaging in rat. Eur. Neuropsychopharmacol. J. Eur. Coll. Neuropsychopharmacol. 26 (3), 518–531.
Pan, W.J., Thompson, G., Magnuson, M., Majeed, W., Jaeger, D., Keilholz, S., 2011. Broadband local field potentials correlate with spontaneous fluctuations in functional magnetic resonance imaging signals in the rat somatosensory cortex under isoflurane anesthesia. Brain Connect. 1 (2), 119–131.
Pierrel-Sorrentino, R., Raslear, T.G., 1980. Loudness scaling in rats and chinchillas. J. Comp. Physiol. Psychol. 94 (4), 757–766.
Pirttimaki, T., Salo, R.A., Shatillo, A., Kettunen, M.I., Paasonen, J., Sierra, A., Jokivarsi, K., Leinonen, V., Andrade, P., Quittek, S., others, 2016. Implantable RF-coil with multiple electrodes for long-term EEG-fMRI monitoring in rodents. J. Neurosci. Methods 274, 154–163.
Raj, D., Paley, D.P., Anderson, A.W., Kennan, R.P., Gore, J.C., 2000. A model for susceptibility artefacts from respiration in functional echo-planar magnetic resonance imaging. Phys. Med. Biol. 45 (12), 3809–3820.
Schmitter, S., Diesch, E., Amann, M., Kroll, A., Moayer, M., Schad, L.R., 2008. Silent echo-planar imaging for auditory FMRI. Magma 21 (5), 317–325.
Schomer, P.D., 1978. Growth function for human response to large-amplitude impulse noise. J. Acoust. Soc. Am. 64 (6), 1627–1632.
Sheoran, M., Kumar, S., Kumar, A., 2014. Wavelet-ICA based denoising of electroencephalogram signal. Int. J. Inf. Comput. Technol. 4, 1205–1210.
Silva, A.C., Koretsky, A.P., Duyn, J.H., 2007. Functional MRI impulse response for BOLD and CBV contrast in rat somatosensory cortex. Magn. Reson. Med. 57 (6), 1110–1118.
Smith, J.B., Liang, Z., Watson, G.D.R., Alloway, K.D., Zhang, N., 2017. Interhemispheric resting-state functional connectivity of the claustrum in the awake and anesthetized states. Brain Struct. Funct. 222 (5), 2041–2058.
Sommers, M.G., van Egmond, J., Booij, L.H., Heerschap, A., 2009. Isoflurane anesthesia is a valuable alternative for alpha-chloralose anesthesia in the forepaw stimulation model in rats. NMR Biomed. 22 (4), 414–418.
Stenroos, P., Paasonen, J., Salo, R.A., Jokivarsi, K., Shatillo, A., Tanila, H., Grohn, O., 2018. Awake rat brain functional magnetic resonance imaging using standard radio frequency coils and a 3D printed restraint kit. Front. Neurosci. 12, 548.
Sumiyoshi, A., Riera, J.J., Ogawa, T., Kawashima, R., 2011. A mini-cap for simultaneous EEG and fMRI recording in rodents. Neuroimage 54 (3), 1951–1965.
Tomasi, D., Caparelli, E.C., Chang, L., Ernst, T., 2005. fMRI-acoustic noise alters brain activation during working memory tasks. Neuroimage 27 (2), 377–386.

Tustison, N.J., Avants, B.B., Cook, P.A., Zheng, Y., Egan, A., Yushkevich, P.A., Gee, J.C., 2010. N4ITK: improved N3 bias correction. IEEE Trans. Med. Imaging 29 (6), 1310–1320.
Upadhyay, J., Baker, S.J., Chandran, P., Miller, L., Lee, Y., Marek, G.J., Sakoglu, U., Chin, C.L., Luo, F., Fox, G.B., others, 2011. Default-mode-like network activation in awake rodents. PLoS One 6 (11), e27839.
Zaitsev, M., Akin, B., LeVan, P., Knowles, B.R., 2017. Prospective motion correction in functional MRI. Neuroimage 154, 33–42.
Zapp, J., Schmitter, S., Schad, L.R., 2012. Sinusoidal echo-planar imaging with parallel acquisition technique for reduced acoustic noise in auditory fMRI. J. Magn. Reson. Imaging JMRI 36 (3), 581–588.
Zhang, N., Rane, P., Huang, W., Liang, Z., Kennedy, D., Frazier, J.A., King, J., 2010. Mapping resting-state brain networks in conscious animals. J. Neurosci. Methods 189 (2), 186–196.